important in the Pariser-Parr[13] and subsequent derivative semiempirical theories of electronic structure of molecules.[14] It also is the basic parameter in the Hubbard model of solids;[15] for an insulator it is just the band gap. Our whole discussion has been, however, completely independent of a particular theory of electronic structure.

The hardness of a chemical species, then, is half the derivative of its chemical potential with respect to the number of electrons: $2\eta = (\partial\mu/\partial N)_Z$. There seem to be no other acceptable definitions.[16]

Acknowledgment. R. G. Parr thanks the National Science Foundation and the National Institutes of Health for research grants, the University of North Carolina for a Pogue leave, and the Institute for Theoretical Physics at Santa Barbara for gracious hospitality. R. G. Pearson thanks the Department of Energy for a grant (Contract DE A503-76SF00034) used in partial support of this work.

(13) R. Pariser and R. G. Parr, *J. Chem. Phys.*, **21**, 466-471; 767-76 (1953).
(14) This includes all theories of CNDO, NNDO, and MINDO types.
(15) J. Hubbard, *Proc. R. soc. London, Ser. A*, **276**, 238-57 (1963).
(16) The factor of 2 is arbitrary, to create a symmetry between $(I + A)/2$ and $(I - A)/2$.

EPR Study of the Electronic Structure and Dynamic Jahn-Teller Effect in Nickelocenium Cation

M. V. Rajasekharan,[1a] R. Bucher,[1b] E. Deiss,[1c] L. Zoller,[1d] A. K. Salzer,[1d] E. Moser,[1d] J. Weber,[1e] and J. H. Ammeter*[1d]

Contribution from the Institute of Inorganic Chemistry, University of Zürich, Winterthurerstrasse 190, 8057 Zürich, Switzerland, the Swiss Federal Institute of Technology, 8092 Zürich, Switzerland, and the Section de Chimie, Université de Genève, 1211 Genève 4, Switzerland. *Received June 9, 1983*

Abstract: The nickelocenium cation doped with the magnetic isotope ^{61}Ni has been diluted into several diamagnetic host lattices and studied by EPR spectroscopy at low temperatures in polycrystalline samples. From the analysis of the ^{61}Ni hyperfine tensor, supplemented by EHMO and MS-Xα calculations, a quantitative comparison of the covalency and the dynamic Jahn-Teller effects with the related d^7 system cobaltocene has been possible. From line-width studies as a function of temperature we conclude that the line shape at low temperatures (4 K) is mainly due to inhomogeneous broadening effects; the spin-lattice relaxation increasing rapidly at higher temperatures cannot be explained solely by an Orbach mechanism via a closeby upper Kramers doublet in a satisfactory way.

EPR studies of low-spin d^5 and d^7 sandwich compounds give information on the nature of the degenerate or almost degenerate electronic ground state, i.e., on the covalency of the metal-ligand bonds (via spin-density distributions from magnetic hyperfine coupling constants) and on dynamic Jahn-Teller effects (via so called Ham-type reduction factors multiplying orbital angular momentum contributions to the g values).[2] So far the following metallocenes, bisbenzene complexes, and mixed sandwich complexes with varying degrees of substitution of the C_nH_n aromatic rings with either d^5 δ^3 ($^2\Delta$) or d^7 π^1 ($^2\Pi$) type ground states[2] have been studied by EPR:[3] $Fe(Cp)_2^+$,[4] $Mn(Cp)_2$,[5] $Ru(Cp)_2^+$[6] (d^5), $Co(Cp)_2$,[7] $Ni(Cp)_2^+$,[8] $Fe(Cp)(Bz)$,[9] $Co(Cp)(Bz)^+$,[10] $Fe(Bz)_2^+$,[9] and $Co(Bz)_2^{2+}$[10] (d^7, Cp = cyclopentadienyl, Bz = benzene).

In all cases a pronounced dependence of the EPR parameters (g tensor, metal hyperfine tensor) upon the crystalline host lattice or glassy solvent has been observed. Most of the variation could be attributed to changes in the relative weights of the two close lying pseudodegenerate electronic states caused by changes in the low-symmetry components of the solvent fields, but also—to a lesser degree—to variations in the amplitudes of dynamic Jahn-Teller distortions.[11] In this paper we discuss the EPR spectra of the nickelocenium cation.

The nickelocenium cation is isoelectronic with cobaltocene. Magnetic susceptibility measurements yielded similar moments for cobaltocene and nickelocenium salts.[12] EPR measurements[8] further confirmed a d^7 electronic configuration for nickel in this ion. The resulting $^2E_{1g}$ ground state (using D_{5d} notation) or $^2\Pi$ ground state (using $C_{\infty v}$ notation) is Jahn-Teller active. The emphasis in the earlier EPR work[8] was on evaluating the vibronic coupling parameters from an analysis of the g tensor data alone. Absence of any nuclear hyperfine coupling data made necessary

(1) (a) University of Zürich. Present address: Central University Hyderabad, School of Chemistry, Hyderabad-500134, India. (b) Swiss Federal Institute of Technology. Present address: Dr. W. Ingold AG, 8902 Urdorf. (c) University of Zürich. Present address: EIR, 5303 Würenlingen, Switzerland. (d) University of Zürich, Institute of Inorganic Chemistry. (e) Université de Genève, Section de Chimie, 1211 Genève, Switzerland.
(2) See, e.g.: (a) Warren, K. D. *Struct. Bonding (Berlin)* **1976**, *27*, 45. (b) Clack, D. W.; Warren, K. D. *Ibid.* **1980**, *39*, 1 and references therein.
(3) EPR signals attributed to $Rh(Cp)_2$ have also been claimed, see: Keller, H. J.; Wawersik, H. *J. Organomet. Chem.* **1967**, *8*, 185.
(4) (a) Prins, R.; Reinders, F. J. *J. Am. Chem. Soc.* **1969**, *91*, 4229. (b) Prins, R. *Mol. Phys.* **1970**, *19*, 603.
(5) (a) Ammeter, J. H.; Bucher, R.; Oswald, N. *J. Am. Chem. Soc.* **1974**, *96*, 7883. (b) Switzer, M. E.; Wang, R.; Rettig, M. F.; Maki, A. H. *Ibid.* **1974**, *96*, 7669. (c) Ammeter, J. H. *J. Magn. Reson.* **1978**, 30, 299. (d) Robbins, J. L.; Edelstein, N.; Spencer, B.; Smart, J. C. *J. Am. Chem. Soc.* **1982**, *104*, 1882.
(6) (a) Salzer, A. K.; Koelle, U. *J. Organomet. Chem.* **1983**, *243*, C27. (b) Ramakrishna, B. L.; Salzer, A. K.; Koelle, U.; Ammeter, J. H., unpublished.
(7) (a) Nussbaum, M.; Voitländer, J. *Z. Naturforsch., A* **1965**, *20A*, 1411. (b) Ammeter, J. H.; Swalen, J. D. *J. Chem. Phys.* **1972**, *57*, 678. (c) Ammeter, J. H.; Brom, J. M. *Chem. Phys. Lett.* **1974**, *27*, 380. (d) Ammeter, J. H.; Oswald, N.; Bucher, R. *Helv. Chim. Acta* **1975**, *58*, 671. (e) Ammeter, J. H. *J. Magn. Reson.* **1978**, *30*, 299.
(8) (a) Ammeter, J. H.; Oswald, N.; Bucher, R. *Helv. Chim. Acta* **1975**, *58*, 671. (b) Ammeter, J. H. *J. Magn. Reson.* **1978**, *30*, 299.
(9) (a) Nesmeyanov, A. N.; Solodovnikov, S. P.; Vol'kenau, N. A.; Kotova, L. S.; Sinitsyna, N. A. *J. Organomet. Chem.* **1978**, *148*, C5. (b) Rajasekharan, M. V.; Giezynski, S.; Ammeter, J. H.; Oswald, N.; Michaud, P.; Hamon, J. R.; Astruc, D. *J. Am. Chem. Soc.* **1982**, *104*, 2400. (c) Ammeter, J. H.; Michaud, P.; Astruc, D. *Ibid.* **1982**, *104*, 3755. (d) Brintzinger, H.; Palmer, G.; Sands, R. H. *J. Am. Chem. Soc.* **1966**, *88*, 623.
(10) Ramakrishna, B. L.; Koelle, U.; Ammeter, J. H., unpublished.
(11) Ammeter, J. H.; Zoller, L.; Bachmann, J.; Baltzer, Ph.; Gamp, E.; Bucher, R.; Deiss, E. *Helv. Chim. Acta* **1981**, *64*, 1063.
(12) (a) Engelmann, F. *Z. Naturforsch. B: Anorg. Chem., Org. Chem., Biochem., Biophys., Biol.* **1953**, *8B*, 775. (b) Fischer, E. O.; Jira, R. *Ibid.* **1953**, *8B*, 217.

0002-7863/83/1505-7516$01.50/0

Table I. EPR Parameters for the Nickelocenium Ion in Various Host Lattices

sample no.	host lattice	g_x	g_y	g_z	$g_\perp$[a]	δg[b]	A_x[c]	A_y[d]	A_z[d]
1	$Co(Cp)_2SbF_6$	1.645 (3)	1.691 (8)	1.701 (8)	1.668 (5)	0.046 (11)			
2	$Co(Cp)_2AsF_6$	1.837 (3)	1.876 (3)	1.733 (2)	1.857 (3)	0.039 (6)			
3	$Co(Cp)_2BF_4I$	1.894 (2)	1.943 (5)	1.756 (1)	1.919 (3)	0.049 (7)	(−1)	42 (4)	20 (1)
4	$Rh(Cp)_2PF_6$	1.923 (2)	1.966 (2)	1.766 (2)	1.945 (2)	0.043 (4)	(−3)	46.5 (1.0)	18 (1)
5	$Co(Cp)_2BF_4$ II	1.943 (5)	1.986 (2)	1.776 (1)	1.965 (3)	0.043 (7)	(−1)	44 (1)	19 (1)
6	$Co(Cp)_2B(C_6H_5)_4$ I	1.961 (7)	2.004 (3)	1.791 (3)	1.983 (5)	0.043 (10)			
7	$Co(Cp)_2PF_6$	1.973 (1)	2.016 (1)	1.801 (1)	1.995 (1)	0.043 (2)	(0)	47.5 (1.0)	18 (1)
8	$Co(Cp)_2B(C_6H_5)_4$ II	1.979 (3)	2.023 (3)	1.805 (2)	2.001 (3)	0.044 (6)			
9	$Co(Cp)_2B(C_6H_5)_4$ III	1.989 (3)	2.031 (3)	1.812 (2)	2.010 (3)	0.042 (6)			
10	$Co(Cp)_2B(C_6H_5)_4$ IV	1.998 (3)	2.041 (3)	1.834 (2)	2.020 (3)	0.043 (6)			

[a] $g_\perp = 1/2(g_x + g_y)$. [b] $\delta g = g_y - g_x$. [c] $[10^{-4}\ cm^{-1}]$ calculated values (see text); experimental values 0 ± 8. [d] $[10^{-4}\ cm^{-1}]$. Only positive signs for A_y and A_z are consistent with theory (note that g_N for ^{61}Ni is negative).

some a priori assumptions about covalency in the treatment of the *g*-tensor data. In the present work we report ^{61}Ni hyperfine splitting parameters measured in ^{61}Ni-enriched polycrystalline samples of nickelocenium salts diluted in $Co(Cp)_2PF_6$, $Co(Cp)_2BF_4$, and $Rh(Cp)_2PF_6$. This additional piece of experimental information leads to a better characterization of the electronic ground state and of the vibronic coupling. The derived results on covalency and core polarization will be compared with the results of Xα scattered wave calculations performed for different metal-to-ring distances. In addition, we present here polycrystalline line-width data for nickelocenium salts in several host lattices and discuss possible line-broadening mechanisms which will be of interest for electronically degenerate sandwich compounds in general.

Experimental Section

Synthesis. All preparations were carried out under an atmosphere of N_2. Nickelocene ($NiCp_2$) was prepared by the method of Cordes.[13] For the synthesis of $^{61}NiCp_2$, ^{61}Ni powder (70 mg, 80–90% isotopic purity) was converted into $^{61}Ni(H_2O)_6^{2+}$ by oxidation with HCl/H_2O_2 and evaporation of excess acid. An alcoholic solution of $^{61}Ni(H_2O)_6Cl_2$ was treated with NH_3 gas until the solution was nearly colorless and a violet precipitate of $^{61}Ni(NH_3)_6Cl_2$ had formed. This was filtered off and washed with alcohol and diethyl ether. Reaction of the dried nickel salt with sodium cyclopentadienyl as outlined in ref 13 gives 180 mg (80%) of $^{61}NiCp_2$.

$[NiCp]_2BF_4$ was prepared by the reaction between $[Ni_2Cp_3]BF_4$ and diphenylacetylene as described in ref 14, and all other salts were prepared by rapid precipitation from aqueous solutions of $[NiCp_2]BF_4$ with NH_4PF_6, $KAsF_6$, $KSbF_6$, or $NaBPh_4$. $[CoCp_2]BF_4$ was synthesized from $CoCp_2$[13] by oxidation with 40% aqueous HBF_4 in propionic anhydride, precipitation with ether, and recrystallization from H_2O, and the other salts were synthesized by precipitation from aqueous solutions as outlined above. $[RhCp_2]PF_6$ was made by the reaction between an aqueous solution of $RhCl_3 \cdot xH_2O$ containing 5% Me_2SO and thallium cyclopentadienyl as described by Sheats.[15]

Dilute polycrystalline samples of ca. 1% $[NiCl_2]^+$ in $[CoCp_2]^+$ or $[RhCp_2]^+$ as host lattices were prepared by dissolving 15–20 mg of $[NiCp_2]^+$ in 30 mL of propionic anhydride, saturating the solution at room temperature with the appropriate $[CoCp_2]^+$ or $[RhCp_2]^+$ salt, and filtering the solution over a fritted disk topped with cotton wool. On cooling to −30 °C crystals separated which were filtered off and washed several times with ether. Dilute samples of $[^{61}NiCp_2]^+$ were made by dissolving 15 mg of $^{61}NiCp_2$ in 20 mL of acetone, cooling the solution to −30 °C, and adding 1 equiv of $AgBF_4$ or $AgPF_6$ dissolved in 10 mL of acetone. The solutions were saturated at room temperature with the BF_4^- or PF_6^- salts of $[CoCp_2]^+$ and $[RhCp_2]^+$, filtered, and quickly cooled to −80 °C. Microcrystalline material separated, which was filtered off and dried.

EPR Measurements. EPR powder spectra were recorded on a Varian E-line spectrometer operating at X-band frequency. The magnetic field was calibrated with a Varian NMR Gaussmeter, and the microwave frequency was measured with an EIP frequency counter. Temperature control was achieved by using an Oxford Instruments ESR-9 liquid helium cryostat of the continuous flow type. Temperature measurements were made by using a thermocouple situated immediately below the sample tube. Quartz sample tubes were charged in a nitrogen filled glove box and sealed under 500 mbar of He gas in order to improve thermal conductivity. No decomposition was observed for samples sealed this way. EPR spectra were simulated by using a powder simulation program described by Mohos et al.[16] One tenth of the measured line was adopted as the upper limit for the error in the resonance field positions, from which the error estimates for *g* and *A* values were derived.

Table II. Residual Widths at the Low-Temperature Limit of the *x*, *y*, and *z* Components of the Powder EPR Line for $Ni(Cp)_2^+$ in Various Host Lattices

host no.[a]	$W_0(x)$[b]	$W_0(y)$[b]	$W_0(z)$[b]
2	~100	~100	31
3	21	20	17
4	38	45	33
5	20	19	14
7	15	20	16

[a] The numbers refer to Table I. [b] In G.

MX-Xα Calculations. MS-Xα calculations on $Ni(Cp)_2^+$ have been reported in an earlier paper.[17] In this work we give more detailed results, similar to those described in a recent analysis of isoelectronic $Co(Cp)_2$.[18] The standard version of the SCF-MS-Xα method is used; the sphere radii and α parameters have been chosen as described in detail in the two preceding papers.[17,18] Again both spin-polarized (SP) and non-spin-polarized (NSP) calculations were performed in order to investigate core polarization effects on the hyperfine coupling tensor of the ^{61}Ni nucleus.

Results

Typical EPR spectra of nickelocenium diluted in polycrystalline cobaltocenium (or rhodocenium) salts are shown in Figures 1 and 2. Note that at least two chemically inequivalent sites are present in $Co(Cp)_2BF_4$. (Figure 2). Multiplicity of sites is a common observation in electronically degenerate sandwich compounds because of the great sensitivity of the $^2E_{1g}$ and $^2E_{2g}$ ground states to external perturbations caused by asymmetric lattice potentials. In cases where more than one chemically inequivalent site is present, the detailed temperature variation of the spectrum, as well as the expected correlation between g_z and $g_\perp$ values, were used for assigning the *g* values of the different sites. The EPR parameters are collected in Table I.

As expected for systems with near electronic degeneracy, EPR spectra for the nickelocenium salts were observed only at low temperatures (below 70 K in all cases). As the samples are warmed from 4 K, initially only a reduction in intensity is observed due to the changing Boltzman factor. Line broadening then sets in at a characteristic temperature dependent on the host lattice. The temperature variation of the line width for the *z* component of the powder line (full width at half height) is plotted in Figure 3 and compared with analytical curves corresponding to a

(13) Cordes, W. *Chem. Ber.* **1962**, *95*, 3084.
(14) Werner, H.; Ulrich, B.; Salzer, A. *J. Organomet. Chem.* **1977**, *141*, 339.
(15) Sheats, J. E.; Spink, W. C. Proceedings of Third Symposium on Advances in Organometallic Polymers, Dayton, Ohio, 1979.
(16) Daul, C.; Schläpfer, C. W.; Mohos, B.; Ammeter, J. H.; Gamp, E. *Comput. Phys. Commun.* **1981**, *21*, 385.
(17) Goursot, A.; Pénigault, E.; Weber, J. *Nouv. Chim.* **1979**, *3*, 675.
(18) Weber, J.; Goursot, A.; Pénigault, E.; Ammeter, J. H.; Bachmann, J. *J. Am. Chem. Soc.* **1982**, *104*, 1491.

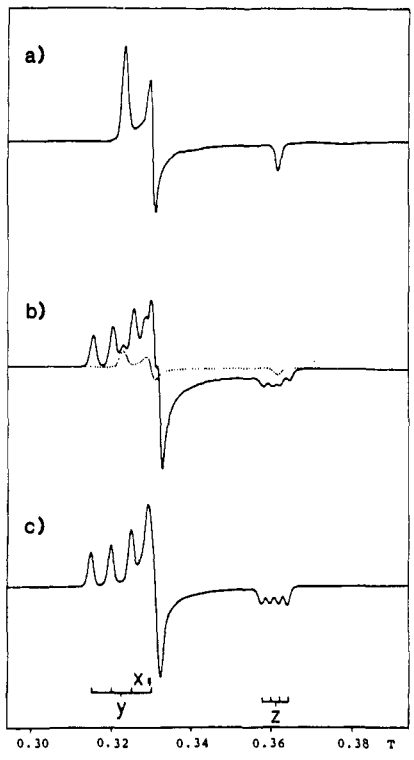

Figure 1. EPR spectrum of $Ni(Cp)_2PF_6$ in $Co(Cp)_2PF_6$ at 4 K (ν = 9.0883 GHz): (a) sample with Ni in natural abundance; (b) experimental spectrum of the ^{61}Ni sample, the appearing extra peaks relative to the calculated spectrum (Figure 1c) originate from a small amount of non-enriched $Ni(Cp)_2PF_6$ (spectrum drawn with dotted lines); (c) computer simulation of spectrum 1b ($A_x = 2 \times 10^{-4}$ cm^{-1}; line width = 1.2 mT).

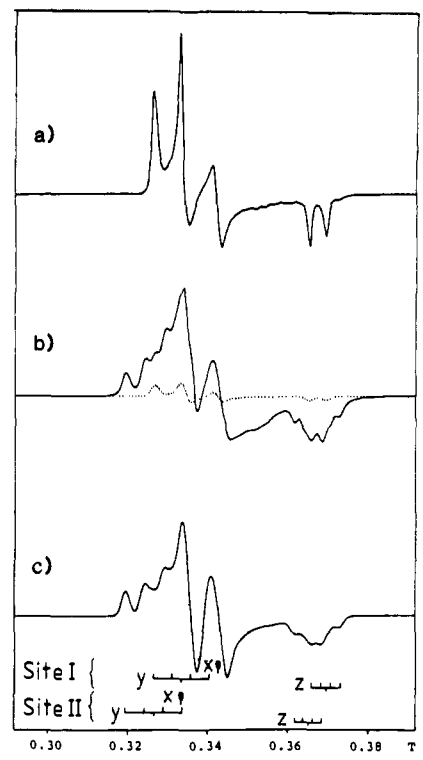

Figure 2. EPR spectrum of $Ni(Cp)_2BF_4$ in $Co(Cp)_2BF_4$ at 4 K (ν = 9.08053 GHz): (a) sample with Ni in natural abundance; (b) experimental spectrum of the ^{61}Ni sample, the appearing extra peaks relative to the calculated spectrum (Figure 2c) originate from a small amount of non-enriched $Ni(Cp)_2BF_4$ (spectrum drawn with dotted lines); (c) computer simulation of Figure 2b ($A_x = 4 \times 10^{-4}$ cm^{-1}; line width = 1.8 mT; intensity ratio of site II:site I = 1:0.7).

least-squares fit to an Orbach-type exponential formula. No additional broadening originating from the addition of ^{61}Ni relative to the non-enriched samples was observed. The limiting line widths at low temperature for the x, y, and z components are given in Table II.

Theoretical Analysis of the EPR Spectra. Model for d^7 Metallocenes in Low-Symmetry Environments. The vibronic MO framework appropriate for the interpretation of the EPR spectra of d^7 metallocenes in low-symmetry environments has been described in earlier papers.[7b,c] In order to eliminate some sign errors and ambiguities and also for the sake of clarity we will repeat here the principal aspects by using a somewhat more transparent notation introduced in a recent theoretical analysis of some electronic properties of cobaltocene.[18] For transition-metal compounds with D_{5d} ($C_{\infty v}$) symmetry, the five highest occupied molecular orbitals having significant metal 3d character can be written as follows,

$$\left.\begin{aligned}\Psi_5 &= c_\pi|d_{yz}\rangle - c_\pi'|\phi_5^L\rangle\\ \Psi_4 &= c_\pi|d_{xz}\rangle - c_\pi'|\phi_4^L\rangle\end{aligned}\right\} e_{1g}(\pi)$$
$$\Psi_3 = c_\sigma|d_{z^2}\rangle - c_\sigma'|\phi_3^L\rangle \quad a_{1g}(\sigma) \qquad (1)$$
$$\left.\begin{aligned}\Psi_2 &= c_\delta|d_{x^2-y^2}\rangle + c_\delta'|\phi_2^L\rangle\\ \Psi_1 &= c_\delta|d_{xy}\rangle + c_\delta'|\phi_1^L\rangle\end{aligned}\right\} e_{2g}(\delta)$$

where $|\phi_n^L\rangle$ are symmetry adapted linear combinations of appropriate ligand atomic orbitals of the cyclopentadienyl rings. For d^7 metallocenes the electronic configuration is $e_{2g}^4 a_{1g}^2 e_{1g}^1$. The resulting $^2E_{1g}$ ground state is Jahn–Teller active. The total Hamiltonian including spin–orbit coupling, orthorhombic potential provided by the host lattice, and vibronic coupling can be written as,

$$\mathcal{H} = \mathcal{H}_{axial}(q) + \mathcal{H}_{rhombic}(q) + \mathcal{H}_{spin\ orbit}(q) + \mathcal{H}_{nucl}(Q) + V'(q,Q) \qquad (2)$$

where q and Q refer to electronic and nuclear coordinates, respectively. An eigenfunction of the first four terms can be approximated as a single Born–Oppenheimer product; thus for the ground Kramers doublet we have[7b]

$$\Psi = \{c|\Psi_4\rangle^{\pm} \mp is|\Psi_5\rangle^{\pm}\}\chi \qquad (3)$$

where $c^2 = {}^1/_2 + {}^1/_2\{1 + (c_\pi^2\zeta/2\delta)\}^{-1/2}$ and $c^2 + s^2 = 1$. χ is a vibrational function, ζ is the one-electron spin–orbit coupling constant for the free ion, and 2δ is the rhombic splitting. The last term in eq 2 produces a vibronic mixing of the ground- and

Table III. Isotropic and Anisotropic Contributions to the ^{61}Ni Hyperfine Tensor of $Ni(Cp)_2^+$ from MS-Xα Calculations Performed for Various Metal-to-Ring Distances[a]

contribution	1.728 A	1.828 A	1.928 A
Isotropic (SP)			
$\rho\uparrow(0) - \rho\downarrow(0)$ total, au	−0.057	−0.118	−0.161
4s	−0.0074	−0.0164	−0.0302
3s	+0.0789	+0.1617	+0.1854
2s	−0.1221	−0.2506	−0.3007
1s	−0.0068	−0.0130	−0.0159
A_F (10^{-4} cm^{-1}, exptl 19 ± 1)	+7.6	+15.8	+21.5
Anisotropic (SP)			
$\rho_M^\pi(4e_{1g}\uparrow)$, %	35.37	33.57	32.59
$P(E_{1g})$, au	3.367	3.652	3.834
$P(E_{2g})$, au	0.140	0.236	0.288
$P(A_{1g})$, au	0.045	0.117	0.167
$2P(A_{2u}) - P(E_{1u})$, au	−0.003	−0.002	−0.000
P_{tot}, au	3.177	3.414	3.592
P_{tot}, 10^{-4} cm^{-1}	−50.6	−54.4	−57.4
Anisotropic (NSP, $4e_{1g}$ MO)			
ρ_M^π, %	36.51	36.73	
$\langle r^{-3}\rangle_{3d}$, au	8.539	8.366	
$P_0 = \rho_M^\pi\langle r^{-3}\rangle_{3d}$, au	3.173	3.411	
$W = P_{tot}/P_0$	1.018	1.110	

[a] For the definition of the different entries, see corresponding Table IX in ref 18 for cobaltocene.

Table IV. Vibronic MO Parameters for $Ni(Cp)_2^+$ Derived from g- and A-Tensor Data

host no.[a]	$k_\parallel$	V	tan α	$x\cdot100$	$x'\cdot100$	c_π^2	ρ[b]	$c_\pi'^2$	A_F[c]
3	0.819 (12)	0.45 (1)	2.80 (7)	0.72 (8)	1.9 (2)	0.45 (4)	0.39 (4)	0.66	19 (3)
4	0.830 (6)	0.49 (1)	3.34 (6)	0.59 (6)	1.4 (1)	0.49 (2)	0.44 (2)	0.62	18 (1)
5	0.821 (6)	0.52 (2)	3.63 (10)	0.65 (7)	1.7 (2)	0.46 (2)	0.40 (2)	0.65	19 (1)
7	0.827 (6)	0.62 (6)	4.98 (20)	0.62 (3)	1.5 (1)	0.48 (2)	0.43 (2)	0.63	20 (1)
average	0.824			0.64	1.6	0.47	0.41	0.64	19

[a] The numbers refer to Table I. [b] $\rho = c_\pi^2 - c_\pi c_\pi' S_\pi$ is the net spin density in the e_{1g} orbital (assuming Mulliken partitioning of overlap density). [c] $A_F = -c_\pi^2 P\kappa$ (isotropic hyperfine coupling constant), 10^{-4} cm^{-1}.

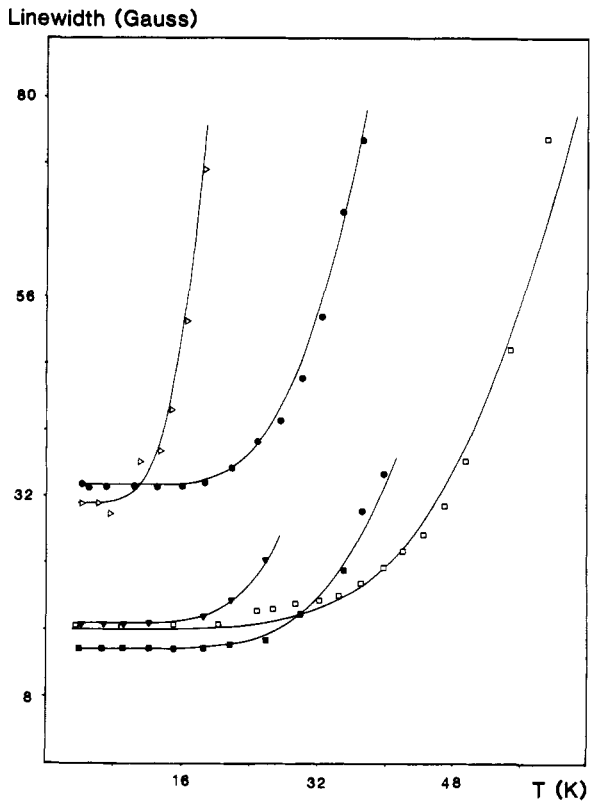

Figure 3. Two-parameter exponential fit $W - W_0 = Ae^{-\Delta E/kT}$ for the temperature dependence of the width of the high-field z line of $Ni(Cp)_2^+$ in various host lattices: (△) $Co(Cp)_2AsF_6$; (▼) $Co(Cp)_2BF_4I$; (●) $Rh(Cp)_2PF_6$; (■) $Co(Cp)_2BF_4II$; (□) $Co(Cp)_2PF_6$.

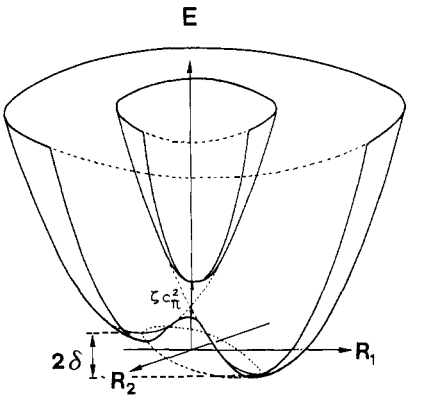

Figure 4. Potential surface for the case of linear JT coupling of an electronic E state with one active e mode (with spin–orbit coupling between the two degenerate electronic E states and with orthorhombic splitting). Q_1 and Q_2 are the two components of the JT active e vibration.

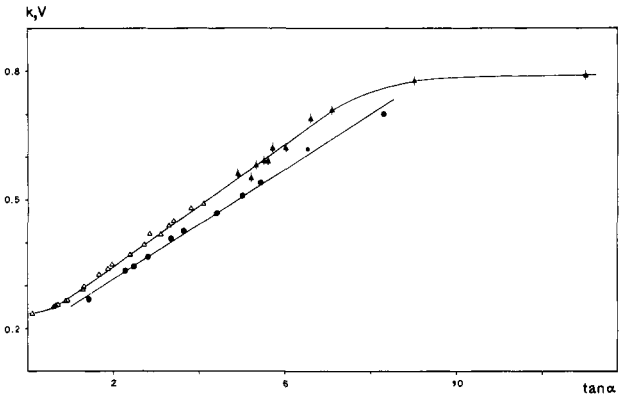

Figure 5. $k_\parallel V$ values for (●) $Ni(Cp)_2^+$, (△) $Co(Cp)_2$, and (▲) alkylated $Co(Cp)_2$ in various host lattices as a function of tan α from g-tensor analysis.

excited-state Kramers doublets so that the ground-state wave function is modified as[7b]

$$\Psi^\pm = c|\Psi_4\rangle^\pm\chi_4 \mp is|\Psi_5\rangle^\pm\chi_5 \qquad (4)$$

The vibrational functions, χ_4 and χ_5, are different, but not orthogonal. A schematic representation of the resulting potential surface in the linear, harmonic coupling case involving a single active mode is shown in Figure 4. The situation corresponds to the case where spin–orbit coupling and rhombic potential are not strong enough to completely quench the vibronic interaction. The wave functions Ψ_μ are delocalized in the circular Jahn–Teller minimum and nonadiabatic, corresponding to a dynamically coupled ground state. For sufficiently large values of δ, i.e., for $\delta \gg \zeta, h\nu$, a static approximation (eq 3), will be sufficient for the evaluation of the EPR parameters.

In order to evaluate the principal components of the g and A tensors, one also has to take into account spin–orbit coupling involving the higher excited states. These terms are relatively small but are necessary, e.g., for an explanation of the nonaxial nature of the g tensor. Including the one-electron d–d excitation $\sigma \rightarrow \pi$ and $\delta \rightarrow \pi$, and using first-order perturbation theory, one can derive the following expressions for the g- and A-tensor elements (eq 5).[18] In the above equations $g_e = 2.0023$ is the electron g value, and $k_\parallel = \langle\Psi_4|l_z|i\Psi_5\rangle\hbar^{-1}$ is the orbital angular momentum reduction factor. It can also be written as $1 - c_\pi'^2(1 - \gamma_\parallel)$ where $\gamma_\parallel = \langle\phi_4^L|l_z|i\phi_5^L\rangle\hbar^{-1}$. V is the vibrational overlap integral, $\langle\chi_4|\chi_5\rangle$, also frequently called vibronic reduction factor or Ham factor.[19,20]

	vibronic coupling case	static limit, $\delta \gg \zeta, h\nu$ (first order in ζ)
g_z	$g_e - 2k_\parallel V\cos\alpha$	$g_e - k_\parallel\zeta/\delta$
$g_\perp = (g_x + g_y)/2$	$(g_e + 5x)\sin\alpha$	$g_e + 5x$
$\delta g = g_y - g_x$	$6(1 + V\cos\alpha)x$	$6x$
A_z	$c_\pi^2P\{2/7 - \kappa - 2V\cos\alpha - 3/7(1 - 3V\cos\alpha)x'\}$	$c_\pi^2P(2/7 - \kappa - 3/7x')$
$A_\perp = (A_x + A_y)/2$	$c_\pi^2P(-1/7 - \kappa + 73/14x')\cdot\sin\alpha$	$c_\pi^2P(-1/7 - \kappa + 73/14x')$
$\delta A = A_y - A_x$	$c_\pi^2P(-6/7 + 45/7x')\cdot(1 + V\cos\alpha)$	$c_\pi^2P(-6/7 + 45/7x')$
tan α	$(c'^2 - s'^2)/2c's'$	$2\delta/(c_\pi^2\zeta)$ (5)

P is the free ion value for $g_e\beta_e g_n\beta_n\langle r^{-3}\rangle_{3d}$ and the product $A_F = -c_\pi^2 P\kappa$ is the Fermi contact term, x and x' are defined in the following way by using the average energy approximation[18]

$$x = c_\pi^2\overline{c_{\sigma,\delta}^2 k_\perp^{\sigma,\delta}}(\zeta/\Delta E)$$
$$x' = c_{\sigma,\delta}^2\zeta/\Delta E \qquad (6)$$

where

$$k_\perp^{\sigma} = 1 - \left(\frac{c_\pi'}{c_\pi}\right)S_\pi - \left(\frac{c_\sigma'}{c_\sigma}\right)S_\sigma + \left(\frac{c_\pi' c_\sigma'}{c_\pi c_\sigma}\right)\frac{\langle\phi_5^L|L_x|\phi_3^L\rangle}{\langle d_{yz}|L_x|d_{z^2}\rangle}$$
$$k_\perp^{\delta} = 1 - \left(\frac{c_\pi'}{c_\pi}\right)S_\pi + \left(\frac{c_\delta'}{c_\delta}\right)S_\delta - \left(\frac{c_\pi' c_\delta'}{c_\pi c_\delta}\right)\frac{\langle\phi_5^L|L_x|\phi_2^L\rangle}{\langle d_{yz}|L_x|d_{x^2-y^2}\rangle} \qquad (7)$$

S_π, S_σ, and S_δ are overlap integrals for π, σ, and δ molecular orbitals, respectively. $\bar{\Delta E}$ is the average value of the $\sigma \rightarrow \pi$ and $\delta \rightarrow \pi$ excitation energies. Note that the different signs in eq 7 originate from the fact that the e_{2g} orbitals are bonding and the e_{1g} and the a_{1g} orbitals antibonding and that the ligand coefficients c_λ' in expression 1 have been chosen positive.[21]

In the above formalism one neglects multiplet splittings and contributions from quartet excited states. The effects of these corrections were investigated in the case of cobaltocene[18] (for which an analyzed ligand field spectrum is available) and were found to make only minor contributions to g and A values. We will therefore neglect these effects which can be expected to be even smaller in $Ni(Cp)_2^+$ than in $Co(Cp)_2$ because of the smaller d character of the open shell and because of the larger d–d splittings.

MS-Xα Calculations. Orbital energies, orbital charge distributions, wave-function contours, and optical transition energies have been given in detail in ref 17. Here we restrict ourselves on the presentation of the hyperfine coupling parameters relevant for the theoretical analysis of the EPR data. As in the case of cobaltocene[18] we give in Table III all the quantities needed for a theoretical prediction of the isotropic and anisotropic contributions to the ^{61}Ni hyperfine tensor, again for three different metal-to-ring distances (cf. Table IX in ref 18). We note a significantly smaller spin density on the metal in nickelocene (37%) than on cobaltocene (57%); in all other aspects the results are very similar and need no further comment.

Determination of Covalency, Static Splitting, and Vibronic Parameters from EPR Data. We have six equations involving g and A tensor elements and seven unknowns, viz., $k_\parallel$, V, tan α, c_π^2, x, x', and κ. However, the large uncertainty in the A_x values (see Table I) forces us to treat A_x as an unknown. Therefore, we sought a consistent solution by an iterative process making use of the interrelationships between c_π, $k_\parallel$, and x/x' from the MO model:

$$k_\parallel = 1 - c_\pi'^2(1 - \gamma_\parallel) \qquad x/x' = c_\pi^2 - c_\pi c_\pi'(S_\pi + T_\sigma) \qquad (8)$$

where

$$T_\sigma = \frac{c_\sigma'}{c_\sigma}\frac{\langle\Psi_5^L|L_x|\Psi_3^L\rangle}{\langle d_{yz}|L_x|d_{z^2}\rangle}$$

and where the small term in S_σ of eq 7 is neglected. S_π, $\gamma_\parallel$, and T_σ were taken from extended Hückel MO's with the help of a program written by Rauk and Ichimura.[22] Because of the unavailability of structural information for nickelocenium salts, we performed two EHMO calculations using for the metal-to-ring distance the values 1.83 (value reported[23] for $Ni(Cp)_2$) and 1.73 Å (value for $Co(Cp)_2$).[24,25] The value of the free-ion parameter, P, was made consistent with the X_α radial function for the e_{1g}* orbital and with the overlap integrals from the EHMO calculation. This is done by assuming the following equation to relate X_α and restricted Hartree–Fock atomic radial integrals,

$$\rho_{X\alpha}\langle r^{-3}\rangle_{X\alpha} = c_\pi^2\langle r^{-3}\rangle_{RHF} \qquad (9)$$

where $c_\pi^2 = \rho_{X\alpha} + c_\pi c_\pi' S_\pi$ and $c_\pi^2 + c_\pi^2 + c_\pi'^2 - 2c_\pi c_\pi' S_\pi = 1$. Using a value of 0.367 au for $\rho_{X\alpha}$ and 8.366 au for $\langle r^{-3}\rangle_{X\alpha}$ obtained from the non-spin-polarized calculation for a metal-to-ring distance of 1.828 Å (Table III), we derived a value of 7.242 au for $\langle r^{-3}\rangle_{RHF}$ and –0.01156 cm^{-1} for P. The free-ion values for P derived from RHF wave functions[26] are –0.01132 cm^{-1} for Ni^{2+} ($3d^8$) and –0.01244 cm^{-1} for Ni^{3+} ($3d^7$). The results shown in Table IV were obtained by using the following parameter set: $S_\pi = 0.105$, $\gamma_\parallel = 0.727$, $T_\sigma = 0.0333$ (corresponding to a metal-to-ring distance of 1.83 Å), and $P = -0.01156$ cm^{-1}. Decreasing the distance by 0.1 Å decreases $k_\parallel$ (increases V) by 2% and increases c_π^2 by 3%, while use of the Ni^{3+} value for P decreases c_π^2 and ρ (increases x') by about 7%. Similarly, if the increase of ca. 10% of P by core polarization effects predicted by MS-Xα ($W = 1.11$, Table III) would be taken into account, c_π^2 and δ would decrease by ca. 7%, thereby reducing the small disagreement of the EPR results with the Xα prediction (41% vs. 37%) further. In view of the uncertainties inherent in our treatment (experimental error, LCAO approximation, neglect of correlation effects) we did not include this refinement in the analysis of Table IV. The calculated values of A_x range between 0 and -3×10^{-4} cm^{-1}, which is consistent with observation. Using the derived value of 0.82 for $k_\parallel$ we recalculated V and tan α for other nickelocenium systems for which only g values are available. Since the radial expectation value $\langle r^{-3}\rangle_{RHF}$ of the Xα calculation was very close to the atomic Hartree–Fock value for Ni^{2+}, we used the spin–orbit parameter ζ for Ni^{2+}. The results are given in Table V.

Table V. tan α, $k_\parallel V$, and x for $Ni(Cp)_2^+$ in Various Host Lattices[a]

host no.[b]	tan α	$k_\parallel V$	$x\cdot 100$	$2\delta_0$[c]
1	1.43 (3)	0.263 (10)	0.65 (17)	0.42
2	2.27 (8)	0.334 (12)	0.53 (13)	0.67
3	2.80 (7)	0.368 (10)	0.72 (8)	0.83
4	3.34 (6)	0.410 (7)	0.58 (3)	0.99
5	3.6 (2)	0.428 (17)	0.65 (7)	1.1
6	4.4 (5)	0.47 (5)	0.63 (12)	1.3
7	5.0 (2)	0.51 (2)	0.62 (3)	1.5
8	5.4 (2)	0.54 (2)	0.65 (3)	1.6
9	6.5 (7)	0.62 (7)	0.63 (6)	1.9
10	8.3 (6)	0.70 (5)	0.64 (5)	2.4

[a] Using a $k_\parallel$ value of 0.82 (the average value derived from a combined analysis of g and A values for four systems) (see Table III). [b] The numbers refer to Table I. [c] $2\delta_0 = c_\pi^2\zeta$ tan α, with $c_\pi^2 = 0.47$, $\zeta = 0.63 \times 10^3$ cm^{-1}.

Discussion

Vibronic Coupling, Covalency, and Core Polarization. The arguments in favor of a vibronic delocalization mechanism as illustrated in Figure 4 can be summarized as follows: First, a static model will require an unreasonably small covalency reduction factor ($k_\parallel \sim 0.2$) or too large initial splitting of the degenerate level ($2\delta \sim 3000$ cm^{-1}) in order to explain the observed g tensor. Second, coexistence of several minima in the Jahn–Teller valley would be possible only in the presence of rather large second-order or anharmonic terms in the effective Hamiltonian.[19] The smooth variation of V with tan α as shown in Figure 5 for both nickelocenium and cobaltocene would be difficult to account for in that case. Vibronic delocalization implies that the Jahn–Teller stabilization energy (E_{JT}) and the effective frequency ($h\nu$) of the

(19) (a) Englman, R. "The Jahn Teller Effect in Molecules and Crystals"; Wiley: New York, 1972. (b) Sturge, M. D. *Solid State Phys.* **1967**, *20*, 91. (c) Bersuker, I. B. *Sov. Phys.-JEPT. (Engl. Transl).* **1963**, *16*, 933.
(20) Ham, F. S. *Phys. Rev.* **1965**, *138*, 1727; **1968**, *166*, 307.
(21) In ref 18 in the corresponding eq 27 the signs are different because the sign of c_L^σ is negative there, while our c_σ' here is positive.
(22) Ichimura, H.; Rauk, A. *J. Chem. Phys.* **1973**, *59*, 5720.
(23) Hedberg, L.; Hedberg, K. *J. Chem. Phys.* **1970**, *53*, 1228.
(24) Bünder, W.; Weiss, E. *J. Organomet. Chem.* **1975**, *92*, 65.
(25) (a) Hedberg, A. K.; Hedberg, L.; Hedberg, K. *J. Chem. Phys.* **1975**, *63*, 1262. (b) Almenningen, A.; Gard, E.; Haaland, A.; Brunnvoll, J. *J. Organomet. Chem.* **1976**, *107*, 273. (c) Haaland, A. *Acc. Chem. Res.* **1979**, *12*, 415.
(26) Goodman, B. A.; Raynor, J. B. *J. Inorg. Nucl. Chem.* **1970**, *32*, 340.

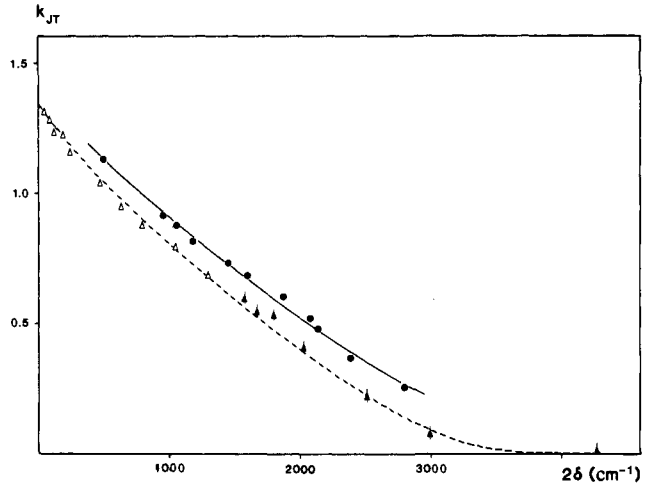

Figure 6. Jahn–Teller coupling constant k_{JT} as a function of 2δ for an assumed frequency of $h\nu = 678$ cm^{-1}: (●) $Ni(Cp)_2^+$, (△) $Co(Cp)_2$, and (▲) alkylated $Co(Cp)_2$ in various host lattices.

coupling mode are of comparable magnitude. The three possible dominant active vibrations for d^7 metallocenes have been discussed in earlier publications.[7e,9b] On the basis of extended Hückel calculations of the potentials for finite distortions along these modes for the case of cobaltocene we have arrived at the following ratios for the individual Jahn–Teller coupling strengths ($k_{JT} = (2E_{JT}/h\nu)^{1/2}$) of the three modes, viz., C–C stretch, C–C–C in-plane bending, and ring torsion: 0.79:0.35:1. Within a linear harmonic single mode coupling approximation one can use the V and tan α values of Table V and Figure 5 to evaluate the variation of k_{JT} with δ. This has been accomplished by a complete diagonalization of the Hamiltonian in eq 2 within a basis of 30 vibrational functions.[7b] The variation of V with k_{JT} is calculated for a large range of δ and ν values. From plots as given in Figures 8 and 9 in ref 9b for an assumed frequency of 678 cm^{-1} we have calculated k_{JT} and δ for each point of Figure 5, and the results are represented in Figure 6, again together with the corresponding plot of cobaltocene and ring-substituted derivatives.[7e] Similar pictures resulted for alternative choices of the frequency of the active mode: for higher frequencies somewhat lower values for k_{JT} were obtained.[35] It is seen that the Jahn–Teller coupling parameter is a strongly decreasing function of the rhombic splitting δ for both d^7 metallocenes considered, consistent with the increase of the vibronic reduction factor with tan α shown in Figure 5. This gradual decrease of k_{JT} with δ has been interpreted recently (ref 11, Figure 13), in terms of pseudomechanical (van der Waals type) lattice potentials acting on the potential surface of the JT active metallocene, whereby only the subspace of the chosen effective e_2 coupling mode is taken into consideration.

From both Figures 5 and 6 it is evident that vibronic coupling effects on the magnetic ground-state properties are significant, as long as the external asymmetric field 2δ is below ca. 3000 cm^{-1}, i.e., 4 quanta of the active vibrational mode. It is also evident that both metallocenes considered are extremely similar in this respect: The differences in Figures 5 and 6 probably originate from the small (ca. 10%) differences of spin–orbit coupling and possibly of the frequenci(es) of the active mode(s); the difference in Figure 6 is probably not significant in view of the uncertainties of $k_{\parallel}$, c_π^2, ζ, and $h\nu$ being all of the same order of magnitude as the resulting difference of the k_{JT} vs. 2δ plot. It is somewhat amusing to observe that in the limit of $\delta \to 0$, i.e., for the free molecule in both d^7 systems, $k_{JT}^2 \approx 2.0$, i.e., the Jahn–Teller energy E_{JT} takes (within experimental error) just the amount of one vibrational quantum of the active mode. It is important to note that this result remains valid in spite of the fact that the assignment of the active mode(s) cannot be solved unambiguously at this stage.

Coming to the question of covalency, it is seen from Table IV that the $k_{\parallel}$ and c_π^2 values obtained in different host lattices are almost identical within experimental error, having average values 0.82 and 0.47, respectively. The corresponding values for $Co(Cp)_2$ are 0.79 and 0.67.[18]

The highest occupied molecular orbital of $Ni(cp)_2^+$ is therefore much more delocalized than in $Co(Cp)_2$. This is also borne out by our extended Hückel and Xα results which place the unpaired electron in a ligand-dominated molecular orbital. The Xα values for the e_{1g}* electron density ($\rho_{X\alpha}$) within the metal sphere are 57% for $Co(Cp)_2$[18] and 37% for $Ni(Cp)_2^+$. These values have to be compared with the partial Mulliken population of 58% and 41% respectively for $Co(Cp)_2$ and $Ni(Cp)_2^+$ derived from EPR data. As in the case of $Co(Cp)_2$ we find good agreement between experiment and Xα prediction for covalency in the HOMO. The spin-density distribution had also been investigated earlier by proton and ^{13}C NMR studies performed for $Co(Cp)_2$[27] and $Ni(Cp)_2^+$[28] as well as on ring-alkylated derivatives.[29] The ^1H contact shift of +105 ppm[28] is almost twice as large as the corresponding value of $Co(Cp)_2$ of +56 ppm, in qualitative agreement with the ratio of the total ligand spin densities derived from Xα (63% vs. 43%) or from EPR (59% vs. 42%). Also the absolute values of the proton shifts are in the expected range, if a McConnell-type mechanism is assumed to be predominant.[27] Quantitative agreement cannot be expected in view of the approximations necessary for an interpretation of isotropic NMR contact shifts in terms of spin-density distributions alone.[27]

Unlike c_π^2 and ρ, the reduction factor, $k_{\parallel}$, turns out to be *not* a good measure for covalent delocalization. This is due to the fact that $k_{\parallel}$ includes two contributions, viz., orbital angular momentum of the d-orbital fraction and that of the ligand (mainly carbon 2p) fraction, $\gamma_{\parallel}$ (see eq 8). The magnitude of $\gamma_{\parallel}$ depends on the extent of s–p hybridization in the ligand part of the e_{1g}* orbital; from the EHMO wave functions we obtained the values 0.66, 0.73, and 0.76 for $Co(Cp)_2^+$, $Ni(Cp)_2^+$, and the free anion Cp^-, respectively. The larger value for $Ni(Cp)_2^+$ compared to that of $Co(Cp)_2$ indicates that the ligand part of the e_{1g}* orbital of $Ni(Cp)_2^+$ is more like that of the free ligand. This increase overcompensates the reduction due to the smaller 3d-orbital coefficient in the molecular orbital since the two contributions happen to have the same sign, leading to almost identical values of $k_{\parallel}$, i.e., 0.79 in $Co(Cp)_2$ and 0.82 in $Ni(Cp)_2^+$.

The Fermi contact contribution (A_F) to hyperfine interaction derived from the EPR data is 19×10^{-4} cm^{-1}. The Xα value for this quantity is very sensitive to the metal-to-ring distance (see Table III). Unfortunately no structural information is available for $Ni(Cp)_2^+$. It is noteworthy that in the case of $Co(Cp)_2$ good agreement between the experimental and the calculated hyperfine tensor was obtained by using the Fermi contact term calculated at the experimental ring–metal distance.[18] If one assumes a similar agreement between experiment and theory for other d^7 metallocenes also, one would predict the metal-to-ring distance in $Ni(Cp)_2^+$ ion to be close to that in the neutral compound. It would be of interest to verify this surprising result by a crystal structure determination. The fact that the A_F values observed in four host lattices do not show appreciable variation can be taken as evidence that the $Ni(Cp)_2^+$ ions do not undergo any gross change in metal–ring distance in these hosts.

Tables IV and V do not show a significant variation of x and x' values among the different host lattices, as expected from the present model. However, there is a wide variation in the accuracy of these numbers for different host lattices due to varying uncertainty in $\delta g = (g_y - g_x)$. (If indeed some lattice dependency of x would exist, one possible reason could be the noncoincidence of g- and A-tensor axes due to unsymmetrical dispositions of Cp rings in the host lattices.) Using the most accurate values of x' we get for the average energy of the $\sigma \to \pi^*$ excitation (eq 6) a value between 3.8 and 4.0 μm^{-1} (assuming $\zeta(Ni^{2+}) = 630$ cm^{-1}[34] and $c_\sigma^2 = 0.9$). The earlier Xα study[17] assuming a metal-to-ring distance of 1.828 Å predicted an average excitation energy of 2.5 μm^{-1} only. Unfortunately, data on d–d transitions in $Ni(Cp)_2^+$ salts are scanty. Optical bands or shoulders have been reported at 2.273 and 2.703 μm^{-1}.[30,31] The peak positions were reported

(27) Rettig, M. F. In "NMR of Paramagnetic Molecules"; LaMar, G. N., Horrocks, DeW. W., Holm, R., Eds.; Academic Press: New York, 1973; p 217 and references therein.
(28) Fritz, H. P.; Köhler, F. H. *Z. Anorg. Allg. Chem.* **1971**, *385*, 22.
(29) Köhler, F. H. *J. Organomet. Chem.* **1976**, *110*, 235.

to be solvent dependent indicating their charge-transfer origin. The d–d bands are presumably masked by higher-energy charge-transfer transitions. More detailed investigations, preferably in single crystals, are needed in this area.

Line Broadening. An examination of Table II shows that the residual widths in the perpendicular (x,y) region are greater than that in the parallel (z) region. The line-width anisotropy increases markedly as the axial limit is approached. In the case of the $Rh(Cp)_2PF_6$ host lattice we have observed that all the lines become broader, leading to an almost complete smearing of the hyperfine splitting, when the sample is finely powdered in a mortar. This effect has also been observed in several samples of $Co(Cp)_2$ in various host lattices. We conclude that the line widths at low temperatures originate mainly in a random distribution of the rhombic distortion (δ), which causes a spread in the g values quite analogous to the case of strain broadening. In this model one would predict that for a given host lattice the anisotropy in these residual widths depends on the distortion parameter α and on the slope of the V vs. tan α curve. The following expressions can be derived for the variation of the parallel and perpendicular resonance field positions with tan α,

$$\frac{dH_{\parallel}}{d\tan\alpha} \sim \frac{1}{g_{\parallel}^2}\left(\cos\alpha\,\frac{dV}{d\tan\alpha} - \frac{V\sin\alpha}{1+(\tan^2\alpha}\right) \quad (10)$$

$$\frac{dH_{\perp}}{d\tan\alpha} \sim \frac{1}{g_{\perp}^2}\,\frac{\cos\alpha}{1+\tan^2\alpha} \quad (11)$$

In the static limit the quantities on the left hand side of eq 10 and eq 11 go to zero, while in the axial limit $dH_{\parallel}/d\tan\alpha$ is proportional to $dV/d\tan\alpha$ and $dH_{\perp}/d\tan\alpha$ tends to infinity because $g_{\perp}$ goes to zero. Because of the two opposing terms in eq 10, $dH_{\parallel}/d\tan\alpha$ will become zero for tan α somewhere between 0 and 1 depending on the positive slope of the V vs. tan α variation. The observed variations of the residual widths in various host lattices (Table II) agree qualitatively with the above predictions, i.e., the z line width is by far the smallest in host lattices, producing small α. Quantitative agreement is not to be expected because the actual spread in the magnitude of δ is not equal in all the host lattices. We therefore conclude that except for large values of tan α, the line width at 4 K is mainly due to inhomogeneous broadening arising from a static modulation of δ rather than due to lifetime broadening.

Lifetime broadening via spin–lattice relaxation becomes significant as the temperature is raised. As in our recent work on Fe(I) sandwich compounds,[9b] the high-temperature widths could be fitted reasonably well to an Orbach-type formula,[32]

$$W - W_0 = Ae^{-\Delta E/kT} \quad (12)$$

where W_0 is the residual width, ΔE is the energy difference between the ground Kramers doublet and the hypothetical excited state participating in the two-level relaxation process, and A is the inverse lifetime of this excited state (see Figure 3). A good quality of the exponential fit could in principle serve as an indication that direct and Raman processes make less important contributions to the spin–lattice relaxation. In the former case the expected variation is proportional to T^2 while in the latter case one expects a T^7 variation.[33] In view of the crudity of the experimental data such a conclusion is not warranted, however. In cases where all the lines are well resolved at higher temperature, the parallel line was found to broaden faster with temperature. This observation seems to rule out the possibilities of a temperature-dependent variation in the spread of δ (a dynamic modulation caused, for example, by a low-frequency ring rotational motion) as the major source of relaxation. The Orbach ΔE values (see Table VI) range from 56 to 166 cm^{-1}. A possible excited state in this range is the upper Kramers doublet. In the dynamic Jahn–Teller model, the energy difference between the two Kramers doublets can be estimated by a Ham-type relation,[19,20]

$$\Delta E = (p^2\zeta^2 + 4q^2\delta^2)^{1/2} \quad (13)$$

where p and q are the vibronic reduction factors for spin–orbit coupling and rhombic distortion, respectively. In the linear single mode coupling approximation, $q = 1/2(1+p)$. Therefore, ΔE should be at least equal to δ $(p = 0, q = 1/2)$. As seen from Table VI the ΔE values are significantly smaller than the estimated δ values, i.e., the q values calculated from Orbach ΔE's via eq 13 are much smaller than 1/2. If the Orbach ΔE's are reliable estimates of the energy separation between the two Kramers doublets, this would mean that either Raman (T^7) contributions to the line width are not negligible or else that a linear single mode approximation is not adequate. However, more direct measurement of ΔE, for example using the inelastic neutron scattering method, as well as more detailed calculations for the multimode coupling case would be necessary for settling this question. At present our accuracy of temperature measurement and our inability to separate rigorously relaxation and inhomogeneous broadening contributions make a more detailed analysis impossible.

Table VI. Orbach Parameters $(\Delta E, A)$ and Rhombic Splitting Parameter (δ) for Selected Systems

host no.[a]	A, G	ΔE, cm^{-1}	δ,[b] cm^{-1}	q[c]
2	3087 (300)	56 (1)	475	0.06
3	2230 (800)	103 (5)	590	0.09
4	3046 (500)	112 (3)	730	0.08
5	2267 (1200)	133 (1)	801	0.08
7	2567 (800)	166 (10)	1046	0.08

[a] Numbers refer to Table I. [b] Calculated from g values assuming $\nu = 678$ cm^{-1} (cf. Figure 6). [c] Calculated from Orbach ΔE via eq 13 for $p = 0$.

Summary and Conclusions

The EPR data for the nickelocenium cation presented in this study can be reconciled with the vibronic MO model introduced earlier for the closely related case of cobaltocene. In spite of a substantial difference in the density distribution of the singly occupied $4e_{1g}^*$ molecular orbital (ca. 57% localized in a metal 3d orbital in cobaltocene vs ca. 40% in nickelocenium) the Jahn–Teller coupling strength turns out to be almost identical in both d^7 metallocenes: the Jahn–Teller stabilization energy equals within experimental error 1 quantum of the active vibrational coupling mode. The earlier hypothesis[7d,e] of a proportionality of the dynamic Jahn–Teller coupling strength to the amount of open-shell density delocalized on the ligand rings thus cannot be maintained. If the dependence of the vibronic reduction factor V on the host lattice is interpreted in terms of pseudomechanical forces exerted by the molecular environment, it turns out that orbital-energy splittings 2δ amounting to ca. 2 vibrational quanta of the active mode are required to reduce the vibronic effects by a factor of 2, while ca. 4 quanta are necessary for quenching the dynamic Jahn–Teller effects by a factor of 10.

Acknowledgment. This work has been supported by the Swiss National Science foundation (project 2.442-0.82).

Registry No. $NiCp_2$, 1271-28-9; ^{61}Ni, 14928-10-0; $Ni(H_2O)_6Cl_2$, 14322-49-7; $Ni(NH_3)_6Cl_2$, 10534-88-0; $[NiCp_2]BF_4$, 65460-78-4; $[Ni_2Cp_3]BF_4$, 37298-59-2; $[CoCp_2]BF_4$, 52314-53-1; $CoCp_2$, 1277-43-6; $[RhCp_2]PF_6$, 1298-45-9; $RhCl_3$, 10049-07-7; $[NiCp_2]^+$, 11091-00-2; $[^{61}NiCp_2]^+$, 87681-21-8; $[CoCp_2]SbF_6$, 87681-22-9; $[CoCp_2]AsF_6$, 87681-23-0; $[CoCp_2]B(C_6H_5)_4$, 12149-53-0; $[CoCp_2]PF_6$, 12427-42-8; sodium cyclopentadiene, 4984-82-1; thallium cyclopentadiene, 34822-90-7; diphenylacetylene, 501-65-5.

(30) Traverso, O.; Rossi, R. *Ann. Univ. Ferrara. Sez.* **1974**.
(31) Borell, O.; Henderson, E. *Inorg. Chim. Acta* **1975**, *12*, 215.
(32) Orbach, R.; Stapleton, H. J. In "Electron Paramagnetic Resonance"; Geschwind, S., Ed.; Plenum Press: New York, 1972; p 121.
(33) Orton, J. "Electron Paramagnetic Resonance: An Introduction to Transition Group Ions in Crystals"; Gordon and Breach: New York, 1969.
(34) Haberditzl, W. "Quantenchemie"; Alfred Hüthig Verlag: Heidelberg, 1979; Bd 4.
(35) Oswald, N. Ph.D. Thesis, ETH Zürich, Nr. 5922, 1977.